Vertical aerosol distribution and mesospheric clouds from ExoMars UVIS

Paul Michael Streeter[1], Graham Sellers[2], Michael J. Wolff[3], J.P. Mason[1], Manish R Patel[2], Stephen Lewis[1], James Andrew Holmes[1], Frank W. Daerden[4], Ian Richard Thomas[5], Bojan Ristic[6], Yannick Willame[7], Cédric Depiesse[6], Ann Carine Vandaele[6], Giancarlo Bellucci[8], and José Juan López-Moreno[9]

[1]Open University
[2]The Open University
[3]Space Science Institute
[4]Royal Belgian Institute for Space Aeronomy BIRA-IASB
[5]Belgian Institute for Space Aeronomy
[6]Royal Belgian Institute for Space Aeronomy
[7]Belgian Institute For Space Aeronomy
[8]Institute for Space Astrophysics and Planetology
[9]Instituto de Astrofisica de Andalucia, IAA-CSIC

November 24, 2022

Abstract

The vertical opacity structure of the martian atmosphere is important for understanding the distribution of ice (water and carbon dioxide) and dust. We present a new dataset of extinction opacity profiles from the NOMAD/UVIS spectrometer aboard the ExoMars Trace Gas Orbiter, covering one and a half Mars Years (MY) including the MY 34 Global Dust Storm and several regional dust storms. We discuss specific mesospheric cloud features and compare with existing literature and a Mars Global Climate Model (MGCM) run with data assimilation. Mesospheric opacity features, interpreted to be water ice, were present during the global and regional dust events and correlate with an elevated hygropause in the MGCM, providing further evidence for the role of regional dust storms in driving atmospheric escape as reported elsewhere. The season of the dust storms also had an apparent impact on the resulting lifetime of the cloud features, with events earlier in the dusty season correlating with longer-lasting mesospheric cloud layers. Mesospheric opacity features were also present during the dusty season even in the absence of regional dust storms, and interpreted to be water ice based on previous literature. The assimilated MGCM temperature structure agreed well with the UVIS opacities, but the MGCM opacity field struggled to reproduce mesospheric ice features, suggesting a need for further development of water ice parameterizations. The UVIS opacity dataset offers opportunities for further research into the vertical aerosol structure of the martian atmosphere, and for validation of how this is represented in numerical models.

Vertical aerosol distribution and mesospheric clouds from ExoMars UVIS

Paul M. Streeter[1], Graham Sellers[1], Michael J. Wolff[2], Jonathon P. Mason[1], Manish R. Patel[1,2], Stephen R. Lewis[1], James A. Holmes[1], Frank Daerden[4], Ian R. Thomas[4], Bojan Ristic[4], Yannick Willame[4], Cédric Depiesse[4], Ann Carine Vandaele[4], Giancarlo Bellucci[5], and José Juan López-Moreno[6].

[1]School of Physical Sciences, The Open University, Walton Hall, Milton Keynes, UK
[2]Space Science Institute, Boulder, Colorado, USA
[3]Space Science and Technology Department, Science and Technology Facilities Council, Rutherford Appleton Laboratory, Oxfordshire, UK
[4]Royal Belgian Institute for Space Aeronomy (IASB-BIRA), Brussels, Belgium
[5]Istituto di Astrofisica e Planetologia Spaziali (IAPS/INAF), Rome, Italy
[6]Instituto de Astrofisica de Andalucía (IAA), Consejo Superior de Investigaciones Científicas (CSIC), Granada, Spain

Key Points:

- Mesospheric water ice clouds were present in ExoMars/UVIS opacity profiles during a global and three regional dust storms
- Mesospheric water ice correlated with elevated hygropause altitude, supporting key role for regional dust storms in driving hydrogen escape
- Perihelion season mesospheric water ice was also present even in the absence of global/regional dust storm activity

Corresponding author: Paul Streeter, `paul.streeter@open.ac.uk`

Abstract

The vertical opacity structure of the martian atmosphere is important for understanding the distribution of ice (water and carbon dioxide) and dust. We present a new dataset of extinction opacity profiles from the NOMAD/UVIS spectrometer aboard the ExoMars Trace Gas Orbiter, covering one and a half Mars Years (MY) including the MY 34 Global Dust Storm and several regional dust storms. We discuss specific mesospheric cloud features and compare with existing literature and a Mars Global Climate Model (MGCM) run with data assimilation. Mesospheric opacity features, interpreted to be water ice, were present during the global and regional dust events and correlate with an elevated hygropause in the MGCM, providing further evidence for the role of regional dust storms in driving atmospheric escape as reported elsewhere. The season of the dust storms also had an apparent impact on the resulting lifetime of the cloud features, with events earlier in the dusty season correlating with longer-lasting mesospheric cloud layers. Mesospheric opacity features were also present during the dusty season even in the absence of regional dust storms, and interpreted to be water ice based on previous literature. The assimilated MGCM temperature structure agreed well with the UVIS opacities, but the MGCM opacity field struggled to reproduce mesospheric ice features, suggesting a need for further development of water ice parameterizations. The UVIS opacity dataset offers opportunities for further research into the vertical aerosol structure of the martian atmosphere, and for validation of how this is represented in numerical models.

Plain Language Summary

The martian atmosphere contains several kinds of aerosol, including dust, water ice, and carbon dioxide ice. The NOMAD/UVIS spectrometer aboard the ExoMars Trace Gas orbiter is able to measure the opacity of the atmosphere at different heights by looking through the atmosphere at the Sun, and these opacities provide information on the vertical aerosol distribution. We present a new dataset of these opacities for one and a half Mars Years, a period including one Global Dust Storm and several smaller regional-scale dust storms. By comparing with a martian climate model and previous work we discuss some noteable features in the UVIS data. We see the presence of high-altitude water ice clouds associated with the Global Dust Storm and several regional dust storms, and find that the lifetime of these cloud layers seems to depend on the seasonal timing of the relevant dust event. These layers also correlate with an elevated higher-altitude water vapour presence, which provides evidence for the role of dust storms at various scales in enhancing hydrogen escape from the atmosphere. The model temperature structure is consistent with the UVIS results, but the model aerosol field shows a need for improvement in its representation of high-altitude water ice.

1 Introduction

Suspended atmospheric aerosols are key components of the martian atmosphere, and their vertical distribution has long been a subject of investigation with orbital observations and modelling. The aerosols found in Mars' atmosphere are mineral dust, water ice, and CO_2 ice, and each have distinct spatiotemporal distributions and radiative effects. Early analytical calculations based on estimated dust sedimentation and diffusion rates alongside orbital observations of a Global Dust Storm (GDS) led to the development of a standard dust profile often used in numerical modelling work, where dust opacity is considered to be constant in a well-mixed bottom layer of the atmosphere before decreasing monotonically at higher altitudes (Conrath, 1974). More recent observations from instruments able to examine the atmospheric limb have revealed a more complex dust vertical structure, including the presence of local dust maxima (detached dust layers) at lower altitudes, particularly during the less dusty aphelion season (e.g. Heavens et al., 2011b; Guzewich, Talaat, et al., 2013), and large plume-like convective dust

structures during GDS (Heavens et al., 2019). Such non-monotonic vertical dust structure is linked to still-debated transport processes involving slope flows and local convective activity (Daerden et al., 2015; C. Wang et al., 2018; Heavens et al., 2015, e.g.), and its representation in Mars Global Climate Models (MGCM) has been shown to have noticeable effects on the thermal structure and circulation (Guzewich, Toigo, et al., 2013). In general, dust appears to be confined below around 20 km during the aphelion season and below 30-50 km during the more active perihelion season (Smith et al., 2013). The presence of dust is also linked to hydrogen escape from the martian atmosphere, which has been shown to be enhanced by atmospheric heating and boosted vertical transport of water from GDS (Chaffin et al., 2014; Heavens et al., 2018) and regional dust storms (J. Holmes et al., 2021).

The distribution of water and CO_2 condensates is tied to the seasonal behaviour of their relevant cloud formations. In general, the formation of water ice clouds requires sufficient presence of water, low enough temperatures for condensation, and cloud condensation nuclei (CCN). The aphelion cloud belt (ACB) is an annual water ice feature visible straddling the tropics during the aphelion season due to the lower atmospheric temperatures, with peak opacity values at around L_S=100° (e.g. Smith, 2008, 2009; Clancy et al., 1996; Mateshvili et al., 2009), with altitudes of around 17-45 km depending on latitude - tending to be higher in the northern tropics than the southern (Smith et al., 2013). ACB opacities have been observed to be higher at 1700 local time than at 1400 local time (Smith, 2009). Another annual water ice feature is the presence of polar hood clouds around both poles from late hemispheric summer to early spring (H. Wang & Ingersoll, 2002), linked to cooler temperatures and the availability of CCN from circumpolar baroclinic dust storms (Cantor et al., 2010). Both polar hood cloud features range from approximately 10-40 km in altitude, with opacity being highly dependent on atmospheric temperature changes (Benson et al., 2010, 2011). Recently however, Clancy et al. (2019) have detected mesospheric (here defined as >40 km) water ice clouds during Mars' perihelion season between 50-90 km altitudes and across the whole of their study's observable range of 50° S-50° N, with a minimum towards lower latitudes.

Lastly, Mars' low atmospheric temperatures enable the characteristically martian phenomenon of CO_2 ice clouds. These features have been detected at high altitudes above the tropics and subtropics, generally in the 65-100 km altitude range in the aphelion season when the atmospheric temperature is particularly low (e.g. Clancy et al., 2019; Aoki et al., 2018; McConnochie et al., 2010; Määttänen et al., 2010; Montmessin et al., 2006); MGCMs are currently unable to replicate these low temperatures, which may be the effect of dynamical phenomena such as gravity waves and thermal tides (e.g. González-Galindo et al., 2011; Spiga et al., 2012). Such phenomena may have to do with the apparent ephemerality of CO_2 ice clouds, which may have lifetimes as low as minutes (Listowski et al., 2014); indeed, while there are now many reported detections, CO_2 ice presence is sparse in retrievals, for example only appearing in less than 1% of Spectroscopy for the Investigation of the Characteristics of the Atmosphere of Mars (SPICAM) mesospheric retrievals (Montmessin et al., 2006). Likewise, stellar occultations from the Imaging Ultraviolet Spectrograph (IUVS) aboard the Mars Atmosphere and Volatile Evolution (MAVEN) spacecraft showed high-altitude (>90 km) CO_2 clouds in only 2 of 32 supersaturated CO_2 profiles, out of a total of 309 stellar occultation profiles (Jiang et al., 2019). Longer-lasting and optically thicker low-altitude (<25 km) CO_2 ice clouds have also been detected in Mars' polar night (Hayne et al., 2012).

The spectrometer instruments aboard the ExoMars Trace Gas Orbiter (TGO), launched in 2016, have already helped contribute to the understanding of martian atmospheric aerosol distribution. Nadir and Occultation for MArs Discovery (NOMAD) (Vandaele et al., 2015) and Atmospheric Chemistry Suite (ACS) (Korablev et al., 2015) are both spectrometer suites aboard TGO and have been observing the martian atmosphere since 2018 in both nadir and solar occultation modes. Aoki et al. (2019) used NOMAD to investigate

the behaviour of water vapour during the 2018 GDS, finding that water vapour presence in the mesosphere (40-100 km) increased substantially during the storm, particularly between 60° S-60° N in the growth stages (L_S=195-220°) and at higher latitudes in the decay stages (L_S=220-260°); the later Mars Year 34 (MY 34) regional dust storm (RDS) had similar effects. Also with NOMAD, Liuzzi et al. (2020) examined the behaviour of water ice clouds during the storm, finding that the storm induced a high-altitude mesospheric water ice layer which rose from 45 km to 80 km rapidly after the GDS inception, as well as greater water ice abundance at local dusk than at dawn. Using ACS, A. A. Fedorova et al. (2020) found increased high-altitude water vapour, ice, and water saturation during the MY 34 GDS period and the regional dust storm. And again with ACS, Stcherbinine et al. (2020) observed a shift in maximum water ice cloud altitudes from 60 km to above 90 km during the GDS.

Total extinction opacity profiles of the martian atmosphere from other instruments have previously provided insights into the vertical aerosol distribution. Solar occultations from the Phobos 2 spacecraft provided aerosol profiles for northern spring at the equator, allowing identification of water ice clouds from thermal considerations (Chassefière et al., 1992). Solar occultations from SPICAM have been used to obtain aerosol extinction profiles in the 1-1.7μm range between 10-60 km, enabling constraints on top of the haze layer at 40 km and detection of mesospheric clouds between 50-60 km (A. A. Fedorova et al., 2009). SPICAM's UV channel has also been used to investigate aerosol opacity profiles via solar occultations, showing the seasonal dust behaviour of the atmosphere and the presence of high-altitude detached layers during the 2007 GDS (Määttänen et al., 2013).

This paper describes an opacity profile dataset derived from solar occultations performed by the UV and visible spectrometer (UVIS) (M. R. Patel et al., 2017) on the NOMAD instrument, extending from L_S=180° in MY 34 to the end of MY 35. This period covers one and a half martian years, including the MY 34 GDS, the MY 34 regional dust storm (which began at around L_S=320°), and the non-GDS year of MY 35. The coverage of this dataset therefore offers the opportunity for investigation of the extreme conditions of an equinoctial GDS as well as the more average conditions of a non-GDS martian year. This dataset does not contain retrievals of specific dust and ice opacities or properties, instead providing total extinction opacities which do not distinguish between aerosol types. The advantage of this approach is that it does not introduce bias or errors from the specifics of a full aerosol retrieval process, but provides an accurate measured of overall extinction which can be used to investigate total aerosol structure in the atmosphere. It is also technically simpler, enabling the UVIS opacity profile dataset to be updated almost in real time from UVIS solar occultations, providing a quick and comprehensive overview of the aerosol structure of the martian atmosphere. The structure of this paper is as follows. We first describe the process by which the UVIS opacities are obtained, and the MGCM with data assimilation we later compare the UVIS dataset to. We then examine specific cloud opacity features in the dataset and compare them to the MGCM with data assimilation, and discuss these results in the context of previous work.

2 Methods

2.1 UVIS opacity calculation

The opacity profiles used in this study are taken from a larger retrieval dataset derived from UVIS occultations designed to extract other spectral signatures from the data in addition to total aerosol content. The complete retrieval process is described in detail in M. R. Patel et al. (2021), and briefly summarised here for convenience.

NOMAD solar occultations profiles are used covering the period from MY 34 L_S=160° to MY 35 L_S=360°. Solar occultation profiles are self-calibrating in that the measure-

ments are expressed as a transmission value by considering the average of measurements made above the altitude where UVIS can detect the atmosphere (~120 km) as the reference spectrum. Measurements made below this altitude are then expressed as a transmission using this occultation-specific reference. Transmissions <1% are not considered in this study due to lack of signal. The transmission spectra observed by the instrument at successive tangent altitudes above the surface (Fig. 1, top) are converted into slant opacities by using the Beer-Lambert Law. The slant opacity is calculated over the wavelengths 320–360 nm, chosen in order to avoid the Hartley band of ozone absorption (centred at 255 nm) and the poor performance of the detector at shorter wavelengths (M. R. Patel et al., 2021). The slant density profile (Fig. 1, bottom left) is converted to an associated local density profile following a variant of an established onion peeling process (Auvinen et al., 2002; Quémerais et al., 2006; Rodgers, 2000). Assuming a spherically symmetric atmosphere in the plane of the observations, the line-of-sight path lengths through each of these atmospheric layers are then calculated geometrically to yield opacity profiles (Fig. 1, bottom right). Uncertainties on the vertical profiles are calculated via an analogous method of inversion; due to inherent uncertainties in the observed transmissions, the resultant detection limit of opacity is defined as $\sim 10^{-5}$.

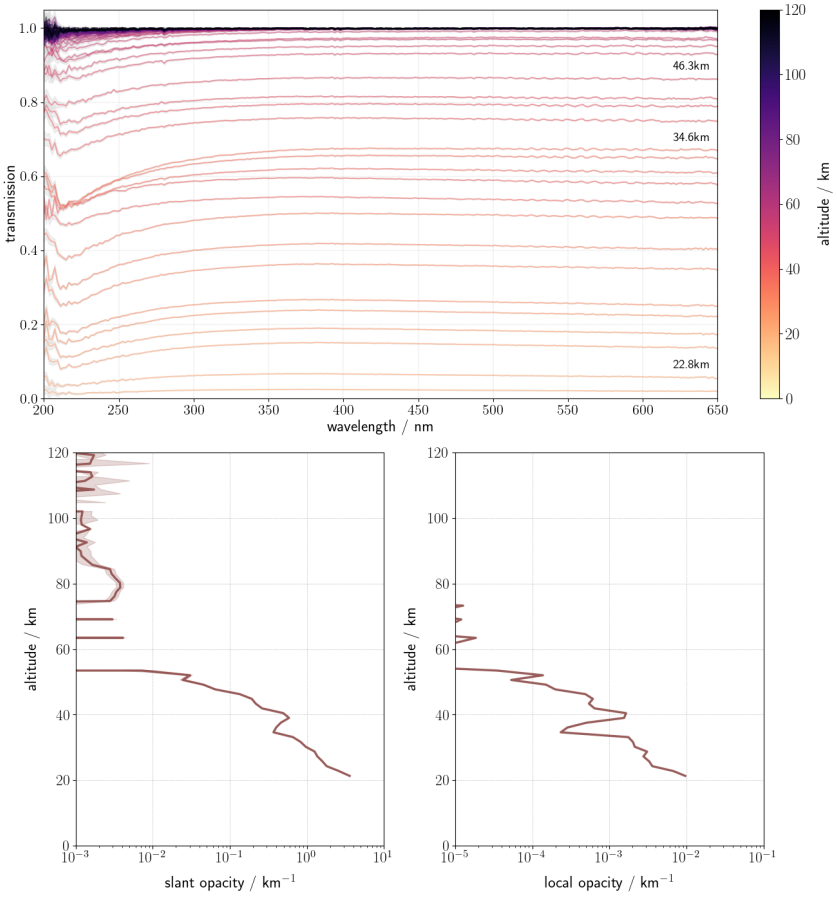

Figure 1. The measured transmission spectra from an example occultation observed on 2018–10–30 at 19:32:49 (UTC) (top). Aerosol slant opacities at 320 nm are extracted from these transmissions using the Beer-Lambert law (bottom left) and an onion-peeling based vertical inversion procedure is conducted on the obtained slant opacities to produce local opacity vertical profiles (bottom right).

2.2 MGCM and assimilation details

For comparison to the UVIS data, the MGCM used is a 4D numerical model which is as a collaborative effort between the Laboratoire de Météorologie Dynamique, the University of Oxford, the Open University, and the Instituto de Astrofísica de Andalucía (Forget et al., 1999). This specific MGCM version uses a spectral dynamical core to solve the primitive equations of fluid dynamics, with a finite-difference scheme along the vertical dimension and a semi-Lagrangian tracer advection scheme (Lewis et al., 2007). The MGCM advects tracers including dust and water using a two-moment scheme with a log-normal size distribution, and at each atmospheric column total column dust optical depth (CDOD) is scaled to match assimilated CDOD observations (Madeleine et al., 2011; P. M. Streeter et al., 2020). The vertical dust distribution is allowed to evolve freely without constraint, with only the CDOD being prescribed. The MGCM uses radiatively active dust with observationally-derived radiative properties (Wolff et al., 2006, 2009). The radiative transfer scheme in the MGCM is robust to within ∼10% error even at the extreme CDOD values measured during the MY 34 GDS (Toon et al., 1989; P. M. Streeter et al., 2020). The MGCM was run with a water cycle using the most recent cloud microphysics package (Navarro et al., 2014), which includes the effects of radiatively active water ice.

The MGCM was run together with a modified version of the Analysis Correction data assimilation scheme (Lorenc et al., 1991), adapted for the case of the martian atmosphere (Lewis et al., 1997, 2007). Retrieved temperature profiles from Mars Climate Sounder (MCS) aboard the Mars Reconnaissance Orbiter (MRO) were assimilated following the technique previously used with this MGCM and assimilation scheme for Thermal Emission Spectrometer (TES) (Lewis et al., 2007; J. A. Holmes et al., 2018) and MCS (J. A. Holmes et al., 2019; Steele et al., 2014) temperatures, while CDOD derived from MCS limb measurements was assimilated to constrain MGCM dust columns as described above (Lewis et al., 2007). The MGCM and assimilation process were the same as previously used for the OpenMARS dataset, which currently extends to MY 32 (J. Holmes et al., 2019).

MCS temperature profiles extend to an altitude of ∼85 km, with a ∼5 km intrinsic vertical resolution (Kleinböhl et al., 2009). MRO's sun-synchronous orbit results in two approximately fixed MCS observation local times, specifically 0300 and 1500 at non-polar latitudes (Zurek & Smrekar, 2007). The MCS retrieval version was v5.2, which incorporates two-dimensional radiative transfer to correct for lateral temperature and aerosol gradients, leading to improved polar retrievals (Kleinböhl et al., 2017). This version was used at all times except for the period of the 2018 GDS, where a reprocessed version (v5.3.2) was used; this reprocessed version incorporated information from additional MCS channels, allowing better retrievals of the high dust opacities of the GDS (Kleinböhl et al., 2020). MCS does not directly retrieve CDOD but provides a derived column product based on extrapolation of retrieved dust profiles. This derived CDOD is reported at infrared wavelengths but the MGCM uses visible wavelengths for dust radiative transfer calculations, and so CDOD values were first converted from 21.6 μm to 670 nm via a conversion factor of 7.3 (Kleinböhl et al., 2011). Dayside equatorial CDOD values were removed prior to assimilation in order to avoid spuriously high values (Montabone et al., 2015), except during the MY 34 GDS (Montabone et al., 2020). As with MCS temperatures, the retrieval version was v5.2 except during the GDS period, when v5.3.2 retrievals were used.

3 Overview of UVIS opacity dataset

The UVIS occultation opacity dataset contains aerosol extinction opacities and slant opacities from L_S=163° of MY 34 to the end of MY 35, at wavelengths in the entire UVIS range from 200-650 nm. Occultations primarily occur at mid-high latitudes and are sparser

in the tropics. Included with the dataset are quality control flags for transmission, which decreases towards the surface of the planet.

Figs. 2 and 3 display the UVIS opacity profiles for each hemisphere for MY 34 and MY 35 respectively, averaged between the wavelengths 320–360 nm, together with the total aerosol opacity field in the MGCM with assimilation (obtained by summing dust and water ice opacities at 670 nm) and the temperature field from the same. UVIS profiles were cut off at low altitudes where transmission fell below 1% and above 100 km altitude (where noise begins to dominate), and the MGCM data was masked to match the times and locations of the UVIS profiles. It should be noted that the constantly varying latitude of the observations means that interpretations must be made carefully, as observed changes in the plots could be due to temporal changes, latitudinal changes, or both. This also applies to local solar time of the occultations, which are always at either the sunrise or sunset terminator.

What follows is a brief description of some features of particular note in the UVIS profiles based on Figs. 2 and 3; further discussion and interpretation can be found in the next section. The MY 34 profiles cover the period of the MY 34 GDS, which began at L_S=185˚ and had decayed to climatological background dust levels by L_S=270˚ (Kass et al., 2019). The GDS signal is clearly visible in Fig. 2 at L_S=200˚, when opacity levels increase between 30-70 km immediately before an extended gap in data due to orbital geometry. After the gap, opacities are once again low above 40 km until L_S=215˚, when a high-altitude layer of high opacity appears between 70-80 km. This high-altitude layer persists until approximately L_S=280˚, decaying in altitude from up to 80 km to around 40-50 km and present even at the northern and southern latitudes of 60˚. Also present are high opacities at lower altitudes, up to 30 km, over roughly the same period. Another high opacity layer is present between 40-60 km around L_S=290-310˚. The MY 34 regional dust storm began at approximately L_S=320˚, correlating with enhanced opacities in the UVIS profiles up to 80 km. Finally, there was high opacity observed at L_S=350-355˚up to approximately 60 km.

MY 35 was a martian year without a GDS. The aphelion season (L_S=0-180˚) is characterised by low opacities above 50 km and high opacity layers at altitudes of 10-50 km. In general there is a low-level opacity feature throughout this period extending to 20-30 km, and sporadic higher-altitude detached features at 40-50 km, most notably around L_S=90-100˚ and L_S=110-135˚ in Fig. 3. The advent of the dustier perhileion season from around L_S=150˚ brings with it an elevation of the lower atmosphere opacity layer, from 20 km at L_S=90˚ to 30-40 km at L_S=190˚. High-altitude opacity layers are visible between 50-70 km throughout L_S=200-270˚. A regional dust storm began at L_S=225˚, correlating with a high-altitude opacity layer appearing at 70 km at L_S=230˚ and decaying to 50 km by L_S=255˚.

4 Discussion

The previous section briefly described particularly notable opacity features in MY 34 and MY 35 as visible in the UVIS dataset. This section explores several of these features in greater detail and provides interpretations regarding their nature by way of more hemispherically-focused analysis, comparison with the MGCM, and comparison with existing literature.

4.1 High-altitude clouds during GDS and regional dust storms in MY 34 and MY 35

The high-altitude opacity features described during the MY 34 GDS are water ice clouds, as noted in published NOMAD and ACS studies. Both Liuzzi et al. (2020) (NOMAD) and Stcherbinine et al. (2020) (ACS) performed retrievals of water ice for the GDS

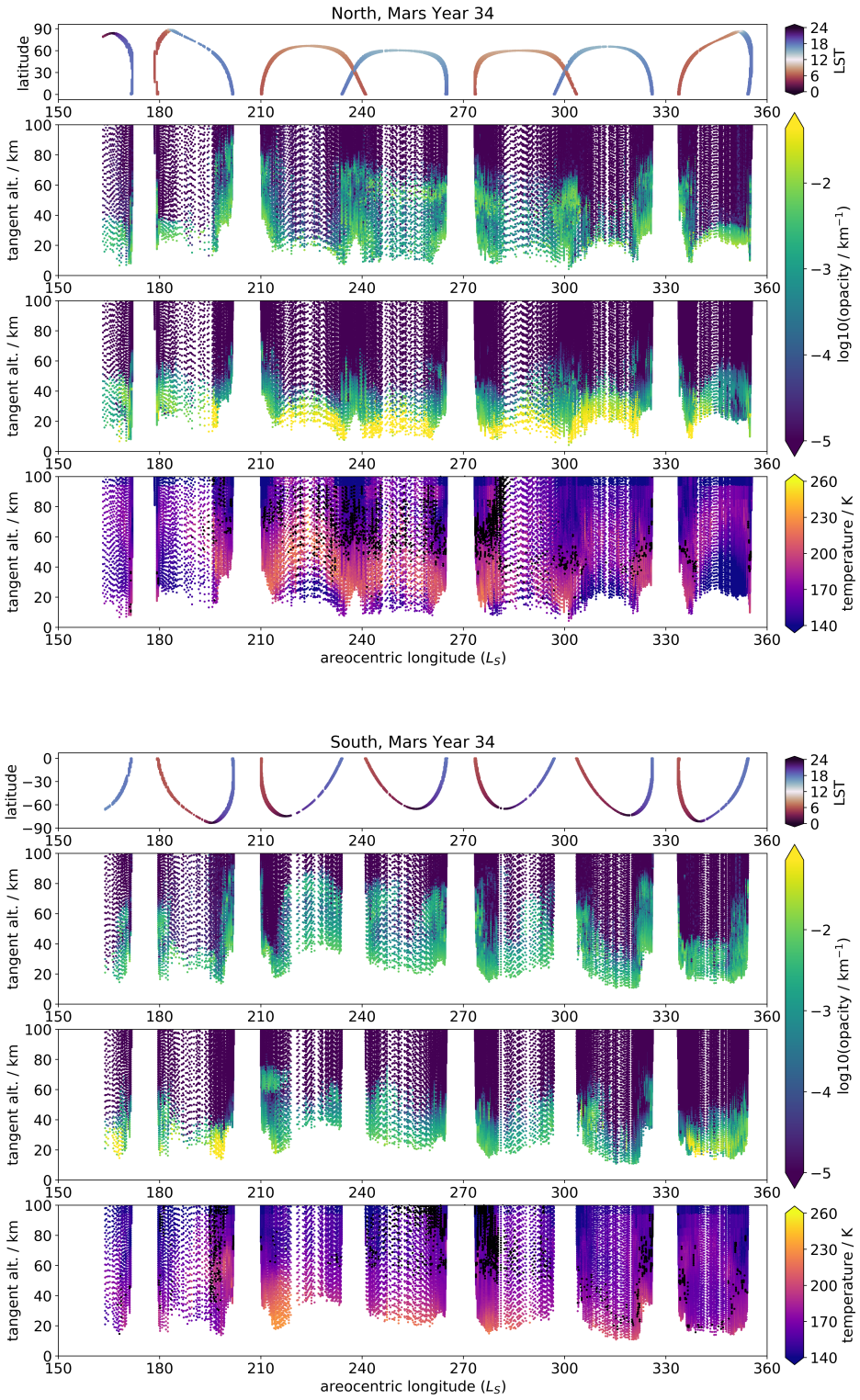

Figure 2. For MY 34 in the northern hemisphere (top four plots) and southern hemisphere (bottom four plots), from top to bottom: UVIS occultation latitude and local solar time distribution; UVIS occultation opacity profiles at 320–360 nm; total (dust + water ice) opacity profiles from the MGCM run with assimilation, matched to the same locations as the UVIS occultations; atmospheric temperatures from the MGCM run with assimilation, matched to the same locations as the UVIS occultations, and overlaid with black dots indicating the approximate location of the hygropause in the MGCM water vapour field, defined here as 70 ppmv (J. Holmes et al., 2021).

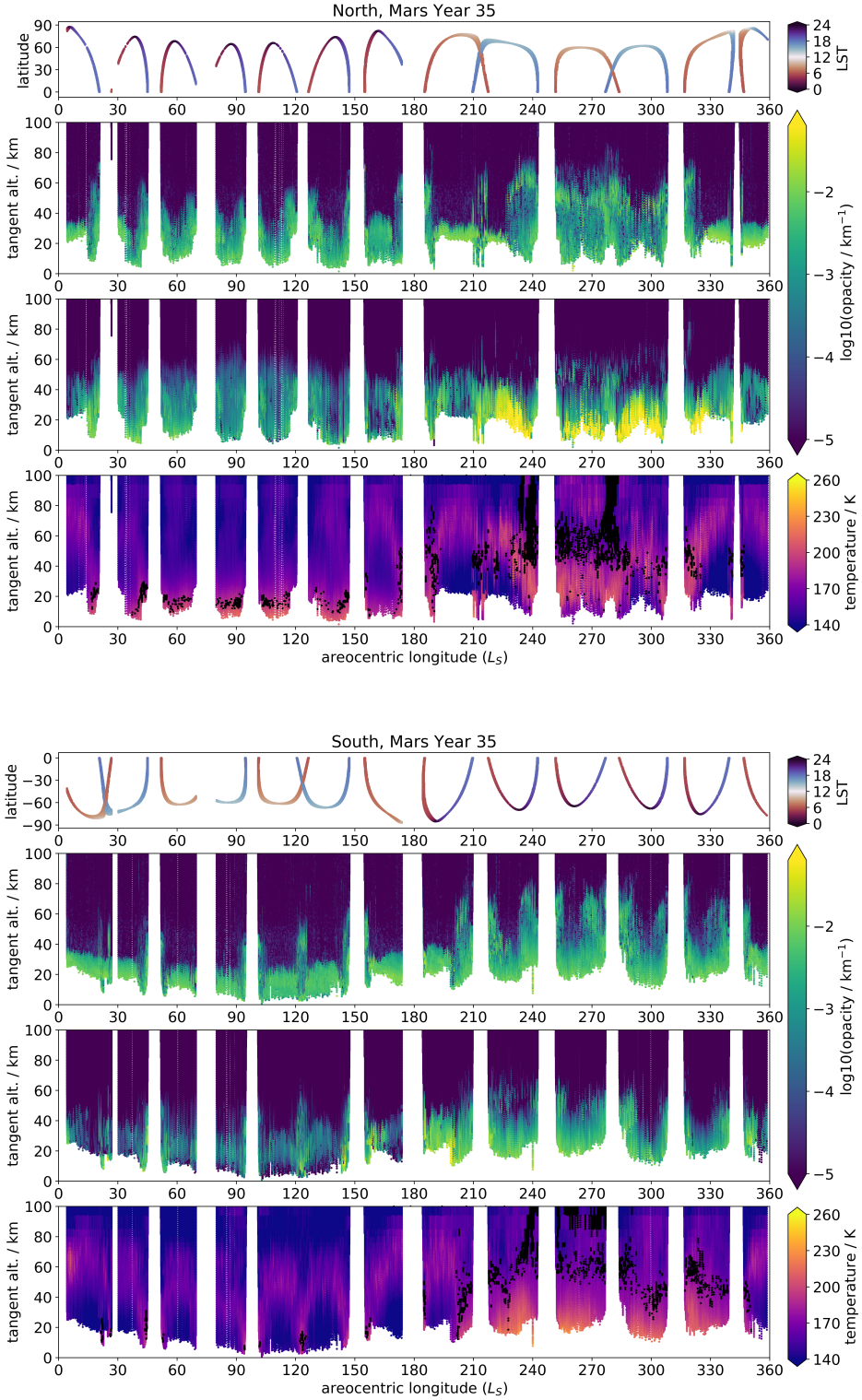

Figure 3. Same as Fig. 2 for MY 35.

period, finding a rise in altitude of a water ice cloud layer from 45-60 km prior to the GDS to 80-90 km during the height of the GDS at L_S=200° which then decayed in altitude to around 50 km as the GDS decayed. Liuzzi et al. (2020) also extended their analysis to the regional dust storm which occurred later in MY 34, beginning at around L_S=320°, and found an increase in dust abundance up to 50 km and water ice abundance up to 80 km. The detachment between these two aerosol kinds is visible in Fig. 2, which shows a separation between a high opacity layer extending to 50 km and one present at 70-80 km. This high-altitude layer is explained as the boosted atmospheric transport enhancing water transport towards higher latitudes and thus increasing the height of the hygropause (Heavens et al., 2018; A. Fedorova et al., 2018). This high-altitude cloud layer was even present at high latitudes, explained dynamically as the enhanced meridional circulation boosting vapour transport towards those latitudes (e.g. Neary et al., 2020). An elegant aspect of the UVIS total opacity dataset is that despite its simplicity, it also reveals the features observed in full retrievals during the MY 34 GDS and regional storms. Comparison with previous full retrievals and the employment of heuristics based on existing research can therefore aid in interpretation of interesting opacity features in data periods which have not yet been subject to full retrievals. This is discussed next in the context of the "A"-type regional dust storm (Kass et al., 2016) observed in MY 35.

MY 35 experienced an "A"-type regional dust storm beginning at approximately L_S=230° and extending roughly from 60° S-45° N at its maximum extent. Fig. 3 shows that, consistent with the mesospheric water ice clouds observed during the MY 34 regional storm, the MY 35 regional storm inception is correlated with a band of enhanced opacities. In the northern hemisphere, this begins at L_S=230° at around 50 km before rapidly rising to 70 km within 5° L_S, then decaying in altitude down to 40 km by L_S=270°. In the southern hemisphere however the band remains at 60-70 km even by L_S=270°. This asymmetry suggests that the higher atmospheric temperatures and dust loading at this time of year (southern summer) may be responsible for maintaining a mesospheric water ice cloud presence. In both hemispheres the high-altitude water ice cloud presence persists for markedly longer than that associated with the MY 34 regional storm; again, this may have to do with the higher dust content and atmospheric temperatures at this time of year. This water ice cloud presence again indicates a raising of the hygropause, which provides further evidence for the important role of regional-scale dust storms in enhancing water escape from the martian atmosphere (J. Holmes et al., 2021).

Finally, these high-altitude water ice cloud features were compared to the MGCM with assimilation to see how well they are reproduced. Interestingly, the southern hemisphere in Fig. 2 shows that the MGCM does contain a 70 km water ice feature at high southern latitudes between L_S=210-220°of MY 34; a time and location when this is not present in the UVIS data. Throughout the rest of the GDS, there is water ice cloud presence in the MGCM at altitudes up to around 60 km, but not the detached layering at higher altitudes seen in the UVIS data. During the MY 34 regional storm there is some enhanced water ice opacity present around 60-70 km, but of several orders of magnitude less than in the UVIS data. Likewise during the MY 35 regional storm in Fig. 3 there is apparent water ice cloud presence at 60 km at L_S=255°, but again lower abundance than seen in the UVIS opacities.

By contrast, the distribution of MGCM atmospheric temperature field and approximate hygropause altitude match noticeably better with the UVIS aerosol opacities. The gradual decay in atmospheric temperatures during the GDS from L_S=220-300° correlates well with the gradual decay in the height of the mesospheric water ice cloud layer in the UVIS data over the same period; the same is the case for the MY 35 regional storm. Likewise, the spike in atmospheric temperatures following the onset of the MY 34 regional storm at L_S=320° aligns well with the high-altitude water ice cloud layer present in the UVIS data in the same time. As temperatures in the MGCM are calculated by assimilating MCS temperature profiles, this suggests that the failure of the MGCM to repli-

cate the mesospheric water ice may be due to a lack of mesospheric water vapour or CCN, or limitations of the cloud parametrization. However, the approximate hygropause altitude as calculated from the MGCM accords well with the location of the high-altitude cloud layers in the UVIS data, which indicates that the water vapour content in the mesosphere is being reasonably well reproduced by the assimilation. The raising of the hygropause during intense GDS dust loading also agrees with previous observations of the MY 28 GDS (Heavens et al., 2018; A. Fedorova et al., 2018).

As a final note, opacities at the bottom of the datasets are significantly (at least an order of magnitude) higher in the MGCM than in the UVIS dataset during the GDS and after, namely from L_S=210-320° of MY 34. As this is most likely dust at these altitudes (Liuzzi et al., 2020), this would imply that the MGCM is overestimating dust presence at roughly 10-30 km, meaning that (assuming the CDOD value is correct) more of the atmospheric dust within the column is located in the bottom scale height or two of the atmosphere than represented in the MGCM; or else, the CDOD value is being overestimated, possibly from spurious opacities due to water ice cloud presence. This has implications for future representation of vertical dust structure in the MGCM, which may need to be adjusted to show a greater dust presence in the bottom scale height of the atmosphere. Future nadir retrievals of CDOD from NOMAD, in conjunction with MCS and NOMAD profiles, should help to better constrain the atmospheric dust content in this crucial bottom 10 km.

4.2 Aphelion clouds in MY 35

The MY 35 aphelion season is characterised by the presence of high opacity features between 10-50 km in the UVIS opacity profiles, increasing in altitude towards the tropics (Fig. 3). These features tend to occur at higher altitudes in the northern than the southern hemisphere. The omnipresent high opacity layers below 30 km in both hemispheres at this time most likely correspond to combined water ice from the ACB and dust, the former having been observed to extend from 17-45 km and the latter up to 20-30 km at this time of year (Smith et al., 2013). The greater altitudes of high opacity features in the north also accord with the northern tropical ACB having been observed to occur at higher altitudes than in the south (Smith et al., 2013), as well as the fact that the north is the spring/summer hemisphere at this time of year, with resulting greater dust activity.

As well as the omnipresent haze below 30 km, higher-altitude opacity features are also visible in the UVIS opacities. These are more prevalent nearer the tropics, and particularly in the northern hemisphere, but examples are also seen in the south. One especially noticeable such feature occurs in both hemispheres around L_S=200° and extends up to 50 km. The particular visibility of this specific feature may be due to the fact that UVIS occultations occur very close to the equator itself at this time, while they are generally constrained poleward of 30° S and 10° N over this aphelion period. The altitude range of this feature is consistent with the higher altitude range of the ACB (Smith et al., 2013) and is higher than the generally reported altitude range (15-25 km) of detached dust layers (e.g. Heavens et al., 2011a). The MGCM local temperature minimum at 50 km/maximum below 50 km at L_S=200° also suggests the presence of cooling (higher albedo) water ice over warming (lower albedo) dust. However, some detached dust layers have been observed at extremely high altitudes over regions of high topography, for example at 55 km (Clancy et al., 2019) and even up to 75 km with a large (<1000 km) spatial footprint (Heavens et al., 2015), likely connected to topographic forcing (Heavens et al., 2015). This particular feature should therefore be of interest for more detailed future examination.

The MGCM aerosol opacity field generally shows good agreement with the UVIS opacities, capturing the gradual dip in altitude of the sub-30 km opacity layer from L_S=0-90° and then its gradual rise again from L_S=90-180°. The MGCM also aptly reproduces

the high-altitude opacity feature in the southern hemisphere at L_S=120°. However, particularly in the northern hemisphere, the MGCM does appear to overestimate opacities above 50 km and underestimate them below, portraying more of a uniform haze than the sharp structure in the UVIS opacities. This suggests that while the cloud scheme is ably reproducing general seasonal and latitudinal trends, there is room for improvement in representing the vertical structure of the ACB.

4.3 High-altitude clouds during MY 35 perihelion

The mesospheric water ice features present during global and regional dust storms have already been discussed, but the UVIS opacities for MY 35 also show similar features during the perihelion season before the beginning of the MY 35 A-type regional storm at L_S=230°. These features can be seen at mid-high latitudes in both hemispheres around L_S=210°, at approximately 50-80 km (Fig. 3). The northern feature is significantly shorter-lived and at a lower altitude (50 km), while the southern feature extends from L_S=200-220° and 50-80 km. The former appears between approximately 45-70° N and the latter between approximately 30-60° S.

The altitudes of these features are greater than those observed for polar hood water ice clouds (Benson et al., 2010, 2011), but along with their latitudes and season agree well with perihelion mesospheric water ice clouds as detected by Clancy et al. (2019) with CRISM in previous martian years. Clancy et al. (2019) noted a sharp dichotomy in mesospheric (50 km+) water ice presence between the colder aphelion season and the warmer perihelion season, with the vast majority of water ice above 60 km being detected between L_S=160-360°. This perihelion mesospheric water ice showed some clustering around mid-high latitudes in both hemispheres, which is also consistent with the UVIS opacities, though there is an intrinsic bias in these due to the lower frequency of equatorial occultations. By contrast, mesospheric CO_2 ice clouds detected by Clancy et al. (2019) occurred primarily during the colder aphelion season, and at tropical latitudes, consistent with many previous studies of mesospheric CO_2 ice clouds (e.g. Vincendon et al., 2011; McConnochie et al., 2010; Määttänen et al., 2010; Aoki et al., 2018). Interestingly, McConnochie et al. (2010) also identified mesospheric cloud features at twilight at mid-latitudes during the perihelion season, but were unable to conclusively classify high their composition. Drawing from these previous results, therefore, the most consistent explanation for the mesospheric opacity features observed in UVIS data is the presence of water ice clouds.

Finally, the UVIS opacities were compared to the MGCM opacities and temperatures. The detached opacity structures are not reproduced by the MGCM, but the temperature and hygropause structure show supporting evidence that these opacity layers are water ice. In both hemispheres, the approximate altitude of the hygropause roughly doubles (from 20 km to 40 km) from the aphelion season to the perihelion season, boosted by the generally higher atmospheric temperatures. In the southern hemisphere, where this opacity layer is greater in spatial and temporal extent, the hygropause rises from below 20 km to 40-60 km between L_S=200-220°and as occultation latitudes move from 70° S towards the tropics. This matches well with the altitude of the UVIS opacity layers in the southern hemisphere, indicating availability of water for condensation. Likewise in the north, a 40-50 km hygropause in the MGCM is present at the time and location of the northern opacity layer at 50 km.

4.4 A brief note regarding CO_2 ice

As mentioned previously, there have been numerous confirmed detections of CO_2 ice clouds in the martian mesosphere, the majority of which have been at equatorial latitudes during the colder aphelion season (e.g. Vincendon et al., 2011; McConnochie et al., 2010; Määttänen et al., 2010; Aoki et al., 2018). The theorised dynamical origins of

such clouds from the creation of cold pockets by gravity waves and/or thermal tides (e.g. González-Galindo et al., 2011; Spiga et al., 2012) may be related to the calculated short lifespans of such features, which could be as low as minutes (Listowski et al., 2014). The equatorial location and ephemerality of mesospheric CO_2 clouds intrinsically makes identification of such features difficult here, as UVIS occultations are relatively sparse at tropical latitudes and the annual-scale L_S-altitude plots presented here are intended to display spatially and temporally extended features on the order of at least several degrees L_S and several kilometres in depth. Fig. 3 shows no significant aphelion high opacity presence in the southern mesosphere, while there is a little more activity in the north, for example at L_S=15-20°near the equator, which does correlate to a high-altitude temperature minimum in the MGCM. As stated though, the sparse nature of mesospheric CO_2 ice clouds, and their reliance on fine-scale and longitudinally-variable dynamics, makes it difficult to draw inferences in a broad study such as this one. We therefore do not draw conclusions regarding the possible presence of mesospheric CO_2 clouds in the UVIS opacity dataset and leave this to future studies, which may benefit from the dusk/dawn local times of the occultations for better understanding of the nature of these phenomena.

5 Conclusions

This article has presented a new dataset freely available to the martian atmospheric community, consisting of total extinction opacity profiles derived from solar occultations by the ExoMars NOMAD/UVIS instrument for the 320–360 nm spectral range. The dataset contains opacity profiles for the period covering the MY 35 Global Dust Storm and regional dust storm, and the entirety of MY 35, allowing investigation of both the extreme dust loading of a GDS year and of a full typical martian year. Solar occultations occur at local dusk and dawn, allowing research into the vertical opacity structure of Mars' atmosphere at the terminator where interesting day-night transition processes may be occurring.

Key features of interest in the UVIS opacity data at the 320–360 nm range have been identified, interpreted according to context and previous literature, and compared to an MGCM with data assimilation. These include the mid-high latitude mesospheric water ice clouds associated with the high dust loading of the MY 34 GDS and regional dust storm, the seasonally reccurring aphelion cloud belt, and perihelion cloud layers in MY 35 – some associated with regional dust storms, others not. Existing retrievals of aerosols in MY 34 allowed identification of the high opacity layers observed in this study above the high dust loading as water ice, and this enabled the inference of very similar layers above regional dust storms in MY 35 as water ice as well. This analysis validates the UVIS opacity dataset as reproducing the observed mesospheric cloud structure in MY 34 and shows its use for ongoing analysis as UVIS continues to perform solar occultations of the atmosphere. With this simple but extensive dataset combined with reasonable inference, it has been shown that mesospheric water ice cloud is regularly seen above regional-scale dust events, and that the season of such events is linked to the temporal extent of these cloud layers. Earlier storms, like the MY 34 GDS (L_S=185°) and MY 35 A-type storm (L_S=230°), are associated with longer-lived mesospheric cloud layers than later storms like the MY 34 regional dust storm (L_S=320°) and the MY 35 C-type storm (L_S=320°). This implies an important role for regional dust storms in martian atmospheric escape.

MGCMs and data assimilation also provide an important function: on the one hand, they can aid in interpretation of specific opacity features via (for example) comparison of the temperature structure; on the other, the UVIS opacity dataset is a potential tool for validation of MGCM aerosol representation, specifically vertical structure. The utility of assimilating temperatures in particular is that it enables better representation of the real thermal structure and dynamics of the martian atmosphere. This provides a valuable interpretative tool for the UVIS opacities, for example by showing how enhanced

lower atmospheric temperatures and a raised hygropause correlate with high-altitude detached opacity layers in the UVIS data, providing supporting evidence for their interpretation as water ice. In the other direction, it is clear from this analysis that current water ice parametrizations struggle to reproduce perihelion mesospheric clouds. Even during the ACB, when the MGCM shows good agreeement with the UVIS opacities, the observations suggest a more vertically confined and sharper aerosol structure than shown in the MGCM. The UVIS dataset therefore offers a good opportunity for validation of aerosol vertical structure in MGCMs simulating both dust and water ice, and development of improved parametrizations.

Acknowledgments

The NOMAD experiment is led by the Royal Belgian Institute for Space Aeronomy (IASB-BIRA), with Co-PI teams in the United Kingdom (Open University), Spain (IAA-CSIC) and Italy (INAF-IAPS). PMS acknowledges support from the STFC under Grant ST/N50421X/1 and The Open University for a PhD studentship. This work was enabled through UK Space Agency grants ST/V002295/1, ST/P001262/1, ST/V005332/1, ST/S00145X/1 and ST/R001405/1, and this project acknowledges funding by the Belgian Science Policy Office (BELSPO), with the financial and contractual coordination by the ESA Prodex Office (PEA 4000103401, 4000121493), by Spanish Ministry of Science and Innovation (MCIU) and by European funds under grants PGC2018-101836-B-I00 and ESP2017-87143-R (MINECO/FEDER), as well as by the Italian Space Agency through grant 2018-2-HH.0. This work was supported by the Belgian Fonds de la Recherche Scientifique – FNRS under grant number 30442502 (ET_HOME). This project has received funding from the European Union's Horizon 2020 research and innovation programme under grant agreement No 101004052.The IAA/CSIC team acknowledges financial support from the State Agency for Research of the Spanish MCIU through the 'Center of Excellence Severo Ochoa' award for the Instituto de Astrofísica de Andalucía (SEV-2017-0709). US investigators were supported by the National Aeronautics and Space Administration.

Data used in this paper is freely available. UVIS opacity occultation profiles can be found in M. Patel et al. (2021), and the comparison assimilation MGCM data masked to match the times/locations of the UVIS profiles can be found in P. Streeter et al. (2021).

References

Aoki, S., Sato, Y., Giuranna, M., Wolkenberg, P., Sato, T. M., Nakagawa, H., & Kasaba, Y. (2018, March). Mesospheric CO2 ice clouds on Mars observed by Planetary Fourier Spectrometer onboard Mars Express. *Icarus*, *302*, 175–190. Retrieved 2018-02-07, from `http://www.sciencedirect.com/science/article/pii/S0019103516306340` doi: 10.1016/j.icarus.2017.10.047

Aoki, S., Vandaele, A. C., Daerden, F., Villanueva, G. L., Liuzzi, G., Thomas, I. R., ... Lopez-Moreno, J.-J. (2019). Water Vapor Vertical Profiles on Mars in Dust Storms Observed by TGO/NOMAD. *Journal of Geophysical Research: Planets*, *124*(12), 3482–3497. Retrieved 2020-04-19, from `https://agupubs.pericles-prod.literatumonline.com/doi/abs/10.1029/2019JE006109` (_eprint: https://agupubs.onlinelibrary.wiley.com/doi/pdf/10.1029/2019JE006109) doi: 10.1029/2019JE006109

Auvinen, H., Oikarinen, L., & Kyrölä, E. (2002). Inversion algorithms for recovering minor species densities from limb scatter measurements at UV-visible wavelengths. *Journal of Geophysical Research: Atmospheres*, *107*(D13), ACH 7–1–ACH 7–9. Retrieved 2021-03-15, from `https://agupubs.onlinelibrary.wiley.com/doi/abs/10.1029/2001JD000407` (_eprint: https://agupubs.onlinelibrary.wiley.com/doi/pdf/10.1029/2001JD000407) doi: https://doi.org/10.1029/2001JD000407

Benson, J. L., Kass, D. M., & Kleinböhl, A. (2011). Mars' north polar hood as observed by the Mars Climate Sounder. *Journal of Geophysical Research: Planets*, *116*(E3). Retrieved 2021-03-08, from https://agupubs.onlinelibrary.wiley.com/doi/abs/10.1029/2010JE003693 (_eprint: https://agupubs.onlinelibrary.wiley.com/doi/pdf/10.1029/2010JE003693) doi: https://doi.org/10.1029/2010JE003693

Benson, J. L., Kass, D. M., Kleinböhl, A., McCleese, D. J., Schofield, J. T., & Taylor, F. W. (2010). Mars' south polar hood as observed by the Mars Climate Sounder. *Journal of Geophysical Research: Planets*, *115*(E12). Retrieved 2021-03-08, from https://agupubs.onlinelibrary.wiley.com/doi/abs/10.1029/2009JE003554 (_eprint: https://agupubs.onlinelibrary.wiley.com/doi/pdf/10.1029/2009JE003554) doi: https://doi.org/10.1029/2009JE003554

Cantor, B. A., James, P. B., & Calvin, W. M. (2010, July). MARCI and MOC observations of the atmosphere and surface cap in the north polar region of Mars. *Icarus*, *208*, 61–81. Retrieved 2017-05-03, from http://adsabs.harvard.edu/abs/2010Icar..208...61C doi: 10.1016/j.icarus.2010.01.032

Chaffin, M. S., Chaufray, J.-Y., Stewart, I., Montmessin, F., Schneider, N. M., & Bertaux, J.-L. (2014). Unexpected variability of Martian hydrogen escape. *Geophysical Research Letters*, *41*(2), 314–320. Retrieved 2021-05-28, from https://agupubs.onlinelibrary.wiley.com/doi/abs/10.1002/2013GL058578 (_eprint: https://agupubs.onlinelibrary.wiley.com/doi/pdf/10.1002/2013GL058578) doi: https://doi.org/10.1002/2013GL058578

Chassefière, E., Blamont, J. E., Krasnopolsky, V. A., Korablev, O. I., Atreya, S. K., & West, R. A. (1992, May). Vertical structure and size distributions of Martian aerosols from solar occultation measurements. *Icarus*, *97*(1), 46–69. Retrieved 2021-05-28, from https://www.sciencedirect.com/science/article/pii/001910359290056D doi: 10.1016/0019-1035(92)90056-D

Clancy, R. T., Grossman, A. W., Wolff, M. J., James, P. B., Rudy, D. J., Billawala, Y. N., ... Muhleman, D. O. (1996, July). Water Vapor Saturation at Low Altitudes around Mars Aphelion: A Key to Mars Climate? *Icarus*, *122*(1), 36–62. Retrieved 2021-03-08, from https://www.sciencedirect.com/science/article/pii/S0019103596901086 doi: 10.1006/icar.1996.0108

Clancy, R. T., Wolff, M. J., Smith, M. D., Kleinböhl, A., Cantor, B. A., Murchie, S. L., ... Sandor, B. J. (2019, August). The distribution, composition, and particle properties of Mars mesospheric aerosols: An analysis of CRISM visible/near-IR limb spectra with context from near-coincident MCS and MARCI observations. *Icarus*, *328*, 246–273. Retrieved 2019-04-12, from http://www.sciencedirect.com/science/article/pii/S0019103518307851 doi: 10.1016/j.icarus.2019.03.025

Conrath, B. J. (1974, April). *Thermal structure of the Martian atmosphere during the dissipation of the dust storm of 1971.* Retrieved 2017-03-08, from https://ntrs.nasa.gov/search.jsp?R=19740018179

Daerden, F., Whiteway, J. A., Neary, L., Komguem, L., Lemmon, M. T., Heavens, N. G., ... Smith, M. D. (2015, September). A solar escalator on Mars: Self-lifting of dust layers by radiative heating. *Geophysical Research Letters*, *42*(18), 2015GL064892. Retrieved 2017-03-08, from http://onlinelibrary.wiley.com/doi/10.1002/2015GL064892/abstract doi: 10.1002/2015GL064892

Fedorova, A., Bertaux, J.-L., Betsis, D., Montmessin, F., Korablev, O., Maltagliati, L., & Clarke, J. (2018, January). Water vapor in the middle atmosphere of Mars during the 2007 global dust storm. *Icarus*, *300*, 440–457. Retrieved 2021-03-11, from https://www.sciencedirect.com/science/article/pii/S001910351730218X doi: 10.1016/j.icarus.2017.09.025

Fedorova, A. A., Korablev, O. I., Bertaux, J. L., Rodin, A. V., Montmessin, F., Belyaev, D. A., & Reberac, A. (2009, March). Solar infrared occultation observations by SPICAM experiment on Mars-Express: Simultaneous measurements of the vertical distributions of H2O, CO2 and aerosol. *Icarus*, *200*(1), 96–117. Retrieved 2021-05-28, from https://www.sciencedirect.com/science/article/pii/S001910350800393X doi: 10.1016/j.icarus.2008.11.006

Fedorova, A. A., Montmessin, F., Korablev, O., Luginin, M., Trokhimovskiy, A., Belyaev, D. A., ... Wilson, C. F. (2020, January). Stormy water on Mars: The distribution and saturation of atmospheric water during the dusty season. *Science*, *367*(6475), 297–300. Retrieved 2020-04-19, from https://science.sciencemag.org/content/367/6475/297 (Publisher: American Association for the Advancement of Science Section: Report) doi: 10.1126/science.aay9522

Forget, F., Hourdin, F., Fournier, R., Hourdin, C., Talagrand, O., Collins, M., ... Huot, J.-P. (1999, October). Improved general circulation models of the Martian atmosphere from the surface to above 80 km. *Journal of Geophysical Research: Planets*, *104*(E10), 24155–24175. Retrieved 2017-03-08, from http://onlinelibrary.wiley.com/doi/10.1029/1999JE001025/abstract doi: 10.1029/1999JE001025

González-Galindo, F., Määttänen, A., Forget, F., & Spiga, A. (2011, November). The martian mesosphere as revealed by CO2 cloud observations and General Circulation Modeling. *Icarus*, *216*(1), 10–22. Retrieved 2021-03-08, from https://www.sciencedirect.com/science/article/pii/S0019103511003150 doi: 10.1016/j.icarus.2011.08.006

Guzewich, S. D., Talaat, E. R., Toigo, A. D., Waugh, D. W., & McConnochie, T. H. (2013, June). High-altitude dust layers on Mars: Observations with the Thermal Emission Spectrometer. *Journal of Geophysical Research: Planets*, *118*(6), 1177–1194. Retrieved 2017-03-24, from http://onlinelibrary.wiley.com/doi/10.1002/jgre.20076/abstract doi: 10.1002/jgre.20076

Guzewich, S. D., Toigo, A. D., Richardson, M. I., Newman, C. E., Talaat, E. R., Waugh, D. W., & McConnochie, T. H. (2013, May). The impact of a realistic vertical dust distribution on the simulation of the Martian General Circulation. *Journal of Geophysical Research: Planets*, *118*(5), 980–993. Retrieved 2017-03-08, from http://onlinelibrary.wiley.com/doi/10.1002/jgre.20084/abstract doi: 10.1002/jgre.20084

Hayne, P. O., Paige, D. A., Schofield, J. T., Kass, D. M., Kleinböhl, A., Heavens, N. G., & McCleese, D. J. (2012). Carbon dioxide snow clouds on Mars: South polar winter observations by the Mars Climate Sounder. *Journal of Geophysical Research: Planets*, *117*(E8). Retrieved 2020-03-27, from https://agupubs.onlinelibrary.wiley.com/doi/abs/10.1029/2011JE004040 doi: 10.1029/2011JE004040

Heavens, N. G., Cantor, B. A., Hayne, P. O., Kass, D. M., Kleinböhl, A., McCleese, D. J., ... Shirley, J. H. (2015, May). Extreme detached dust layers near Martian volcanoes: Evidence for dust transport by mesoscale circulations forced by high topography. *Geophysical Research Letters*, *42*(10), 2015GL064004. Retrieved 2017-03-08, from http://onlinelibrary.wiley.com/doi/10.1002/2015GL064004/abstract doi: 10.1002/2015GL064004

Heavens, N. G., Kass, D. M., & Shirley, J. H. (2019). Dusty Deep Convection in the Mars Year 34 Planet-Encircling Dust Event. *Journal of Geophysical Research: Planets*, *124*(11), 2863–2892. Retrieved 2020-04-05, from https://agupubs.onlinelibrary.wiley.com/doi/abs/10.1029/2019JE006110 doi: 10.1029/2019JE006110

Heavens, N. G., Kleinböhl, A., Chaffin, M. S., Halekas, J. S., Kass, D. M., Hayne, P. O., ... Schofield, J. T. (2018, February). Hydrogen escape from Mars enhanced by deep convection in dust storms. *Nature Astronomy*, *2*(2),

126–132. Retrieved 2018-02-05, from https://www.nature.com/articles/s41550-017-0353-4 doi: 10.1038/s41550-017-0353-4

Heavens, N. G., Richardson, M. I., Kleinböhl, A., Kass, D. M., McCleese, D. J., Abdou, W., ... Wolkenberg, P. M. (2011a, January). Vertical distribution of dust in the Martian atmosphere during northern spring and summer: High-altitude tropical dust maximum at northern summer solstice. *Journal of Geophysical Research: Planets*, *116*(E1), E01007. Retrieved 2016-10-21, from http://onlinelibrary.wiley.com/doi/10.1029/2010JE003692/abstract doi: 10.1029/2010JE003692

Heavens, N. G., Richardson, M. I., Kleinböhl, A., Kass, D. M., McCleese, D. J., Abdou, W., ... Wolkenberg, P. M. (2011b, April). The vertical distribution of dust in the Martian atmosphere during northern spring and summer: Observations by the Mars Climate Sounder and analysis of zonal average vertical dust profiles. *Journal of Geophysical Research: Planets*, *116*(E4), E04003. Retrieved 2016-10-21, from http://onlinelibrary.wiley.com/doi/10.1029/2010JE003691/abstract doi: 10.1029/2010JE003691

Holmes, J., Lewis, S., & Patel, M. (2019, February). *OpenMARS MY28-32 standard database* [Fileset]. Retrieved 2019-03-29, from https://ordo.open.ac.uk/articles/OpenMARS_MY28-32_standard_database/7352579

Holmes, J., Lewis, S., Patel, M., Chaffin, M., Cangi, E., Deighan, J., ... Vandaele, A. (2021). Enhanced water loss from the martian atmosphere during a regional-scale dust storm and implications for long-term water loss. *Earth and Planetary Science Letters*, *571*, 117109. Retrieved from https://www.sciencedirect.com/science/article/pii/S0012821X21003642 doi: https://doi.org/10.1016/j.epsl.2021.117109

Holmes, J. A., Lewis, S. R., Patel, M. R., & Lefèvre, F. (2018, March). A reanalysis of ozone on Mars from assimilation of SPICAM observations. *Icarus*, *302*, 308–318. Retrieved 2018-02-07, from http://www.sciencedirect.com/science/article/pii/S0019103517302889 doi: 10.1016/j.icarus.2017.11.026

Holmes, J. A., Lewis, S. R., Patel, M. R., & Smith, M. D. (2019, August). Global analysis and forecasts of carbon monoxide on Mars. *Icarus*, *328*, 232–245. Retrieved 2019-04-09, from http://www.sciencedirect.com/science/article/pii/S001910351830664X doi: 10.1016/j.icarus.2019.03.016

Jiang, F. Y., Yelle, R. V., Jain, S. K., Cui, J., Montmessin, F., Schneider, N. M., ... Verdier, L. (2019). Detection of Mesospheric CO2 Ice Clouds on Mars in Southern Summer. *Geophysical Research Letters*, *46*(14), 7962–7971. Retrieved 2021-05-27, from https://agupubs.onlinelibrary.wiley.com/doi/abs/10.1029/2019GL082029 (_eprint: https://agupubs.onlinelibrary.wiley.com/doi/pdf/10.1029/2019GL082029) doi: https://doi.org/10.1029/2019GL082029

Kass, D. M., Kleinböhl, A., McCleese, D. J., Schofield, J. T., & Smith, M. D. (2016, June). Interannual similarity in the Martian atmosphere during the dust storm season. *Geophysical Research Letters*, *43*(12), 2016GL068978. Retrieved 2017-03-09, from http://onlinelibrary.wiley.com/doi/10.1002/2016GL068978/abstract doi: 10.1002/2016GL068978

Kass, D. M., Schofield, J. T., Kleinböhl, A., McCleese, D. J., Heavens, N. G., Shirley, J. H., & Steele, L. J. (2019). Mars Climate Sounder observation of Mars' 2018 global dust storm. *Geophysical Research Letters*, *n/a*(n/a). Retrieved 2020-04-03, from https://agupubs.onlinelibrary.wiley.com/doi/abs/10.1029/2019GL083931 doi: 10.1029/2019GL083931

Kleinböhl, A., Friedson, A. J., & Schofield, J. T. (2017, January). Two-dimensional radiative transfer for the retrieval of limb emission measurements in the martian atmosphere. *Journal of Quantitative Spectroscopy and Radiative Transfer*, *187*, 511–522. Retrieved from http://www.sciencedirect.com/science/article/pii/S0022407316302667 doi: 10.1016/j.jqsrt.2016.07.009

Kleinböhl, A., Schofield, J. T., Abdou, W. A., Irwin, P. G. J., & de Kok, R. J. (2011, July). A single-scattering approximation for infrared radiative transfer in limb geometry in the Martian atmosphere. *Journal of Quantitative Spectroscopy and Radiative Transfer*, *112*, 1568–1580. Retrieved 2017-09-20, from http://adsabs.harvard.edu/abs/2011JQSRT.112.1568K doi: 10.1016/j.jqsrt.2011.03.006

Kleinböhl, A., Schofield, J. T., Kass, D. M., Abdou, W. A., Backus, C. R., Sen, B., ... McCleese, D. J. (2009, October). Mars Climate Sounder limb profile retrieval of atmospheric temperature, pressure, and dust and water ice opacity. *Journal of Geophysical Research: Planets*, *114*(E10), E10006. Retrieved 2016-10-21, from http://onlinelibrary.wiley.com/doi/10.1029/2009JE003358/abstract doi: 10.1029/2009JE003358

Kleinböhl, A., Spiga, A., Kass, D. M., Shirley, J. H., Millour, E., Montabone, L., & Forget, F. (2020). Diurnal Variations of Dust During the 2018 Global Dust Storm Observed by the Mars Climate Sounder. *Journal of Geophysical Research: Planets*, *125*(1), e2019JE006115. Retrieved 2020-03-25, from https://agupubs.onlinelibrary.wiley.com/doi/abs/10.1029/2019JE006115 doi: 10.1029/2019JE006115

Korablev, O. I., Montmessin, F., Fedorova, A. A., Ignatiev, N. I., Shakun, A. V., Trokhimovskiy, A. V., ... Kozlova, T. O. (2015, December). ACS experiment for atmospheric studies on "ExoMars-2016" Orbiter. *Solar System Research*, *49*(7), 529–537. Retrieved 2020-03-26, from https://doi.org/10.1134/S003809461507014X doi: 10.1134/S003809461507014X

Lewis, S. R., Collins, M., & Read, P. L. (1997, May). Data assimilation with a martian atmospheric GCM: an example using thermal data. *Advances in Space Research*, *19*, 1267–1270. Retrieved 2017-03-09, from http://adsabs.harvard.edu/abs/1997AdSpR..19.1267L doi: 10.1016/S0273-1177(97)00280-9

Lewis, S. R., Read, P. L., Conrath, B. J., Pearl, J. C., & Smith, M. D. (2007, December). Assimilation of thermal emission spectrometer atmospheric data during the Mars Global Surveyor aerobraking period. *Icarus*, *192*(2), 327–347. Retrieved 2017-03-09, from http://www.sciencedirect.com/science/article/pii/S0019103507003557 doi: 10.1016/j.icarus.2007.08.009

Listowski, C., Määttänen, A., Montmessin, F., Spiga, A., & Lefèvre, F. (2014, July). Modeling the microphysics of CO2 ice clouds within wave-induced cold pockets in the martian mesosphere. *Icarus*, *237*, 239–261. Retrieved 2020-03-15, from http://www.sciencedirect.com/science/article/pii/S0019103514002140 doi: 10.1016/j.icarus.2014.04.022

Liuzzi, G., Villanueva, G. L., Crismani, M. M. J., Smith, M. D., Mumma, M. J., Daerden, F., ... Patel, M. R. (2020). Strong Variability of Martian Water Ice Clouds During Dust Storms Revealed From ExoMars Trace Gas Orbiter/NOMAD. *Journal of Geophysical Research: Planets*, *125*(4), e2019JE006250. Retrieved 2021-03-09, from https://agupubs.onlinelibrary.wiley.com/doi/abs/10.1029/2019JE006250 (_eprint: https://agupubs.onlinelibrary.wiley.com/doi/pdf/10.1029/2019JE006250) doi: https://doi.org/10.1029/2019JE006250

Lorenc, A. C., Bell, R. S., & Macpherson, B. (1991, January). The Meteorological Office analysis correction data assimilation scheme. *Quarterly Journal of the Royal Meteorological Society*, *117*(497), 59–89. Retrieved 2016-10-25, from http://onlinelibrary.wiley.com/doi/10.1002/qj.49711749704/abstract doi: 10.1002/qj.49711749704

Madeleine, J.-B., Forget, F., Millour, E., Montabone, L., & Wolff, M. J. (2011, November). Revisiting the radiative impact of dust on Mars using the LMD Global Climate Model. *Journal of Geophysical Research: Planets*, *116*(E11), E11010. Retrieved 2016-10-20, from http://onlinelibrary.wiley.com/doi/10.1029/2011JE003855/abstract doi: 10.1029/2011JE003855

Mateshvili, N., Fussen, D., Vanhellemont, F., Bingen, C., Dekemper, E., Loodts, N., & Tetard, C. (2009, July). Water ice clouds in the Martian atmosphere: Two Martian years of SPICAM nadir UV measurements. *Planetary and Space Science*, *57*(8), 1022–1031. Retrieved 2021-03-08, from https://www.sciencedirect.com/science/article/pii/S003206330800336X doi: 10.1016/j.pss.2008.10.007

McConnochie, T. H., Bell, J. F., Savransky, D., Wolff, M. J., Toigo, A. D., Wang, H., ... Christensen, P. R. (2010, December). THEMIS-VIS observations of clouds in the martian mesosphere: Altitudes, wind speeds, and decameter-scale morphology. *Icarus*, *210*(2), 545–565. Retrieved 2021-03-08, from https://www.sciencedirect.com/science/article/pii/S0019103510002939 doi: 10.1016/j.icarus.2010.07.021

Montabone, L., Forget, F., Millour, E., Wilson, R. J., Lewis, S. R., Cantor, B., ... Wolff, M. J. (2015, May). Eight-year climatology of dust optical depth on Mars. *Icarus*, *251*, 65–95. Retrieved 2016-10-19, from http://www.sciencedirect.com/science/article/pii/S0019103515000044 doi: 10.1016/j.icarus.2014.12.034

Montabone, L., Spiga, A., Kass, D. M., Kleinböhl, A., Forget, F., & Millour, E. (2020). Martian Year 34 Column Dust Climatology from Mars Climate Sounder Observations: Reconstructed Maps and Model Simulations. *Journal of Geophysical Research: Planets*, *n/a*(n/a), e2019JE006111. Retrieved 2020-03-25, from https://agupubs.onlinelibrary.wiley.com/doi/abs/10.1029/2019JE006111 doi: 10.1029/2019JE006111

Montmessin, F., Bertaux, J.-L., Quémerais, E., Korablev, O., Rannou, P., Forget, F., ... Dimarellis, E. (2006, August). Subvisible CO2 ice clouds detected in the mesosphere of Mars. *Icarus*, *183*(2), 403–410. Retrieved 2021-03-08, from https://www.sciencedirect.com/science/article/pii/S0019103506001205 doi: 10.1016/j.icarus.2006.03.015

Määttänen, A., Listowski, C., Montmessin, F., Maltagliati, L., Reberac, A., Joly, L., & Bertaux, J.-L. (2013, April). A complete climatology of the aerosol vertical distribution on Mars from MEx/SPICAM UV solar occultations. *Icarus*, *223*(2), 892–941. Retrieved 2017-03-24, from http://www.sciencedirect.com/science/article/pii/S0019103512004952 doi: 10.1016/j.icarus.2012.12.001

Määttänen, A., Montmessin, F., Gondet, B., Scholten, F., Hoffmann, H., González-Galindo, F., ... Bertaux, J. L. (2010, October). Mapping the mesospheric CO2 clouds on Mars: MEx/OMEGA and MEx/HRSC observations and challenges for atmospheric models. *Icarus*, *209*(2), 452–469. Retrieved 2021-03-08, from https://www.sciencedirect.com/science/article/pii/S0019103510002095 doi: 10.1016/j.icarus.2010.05.017

Navarro, T., Madeleine, J.-B., Forget, F., Spiga, A., Millour, E., Montmessin, F., & Määttänen, A. (2014, July). Global climate modeling of the Martian water cycle with improved microphysics and radiatively active water ice clouds. *Journal of Geophysical Research: Planets*, *119*(7), 1479–1495. Retrieved 2017-03-09, from http://onlinelibrary.wiley.com/doi/10.1002/2013JE004550/abstract doi: 10.1002/2013JE004550

Neary, L., Daerden, F., Aoki, S., Whiteway, J., Clancy, R. T., Smith, M., ... Vandaele, A. C. (2020). Explanation for the Increase in High-Altitude Water on Mars Observed by NOMAD During the 2018 Global Dust Storm. *Geophysical Research Letters*, *47*(7), e2019GL084354. Retrieved 2020-04-05, from https://agupubs.onlinelibrary.wiley.com/doi/abs/10.1029/2019GL084354 doi: 10.1029/2019GL084354

Patel, M., Mason, J., Sellers, G., & Holmes, J. (2021, Apr). *Nomad-uvis ozone vertical profile retrievals for mars year 34-35.* The Open University. Retrieved from https://ordo.open.ac.uk/articles/dataset/NOMAD-UVIS_ozone

_vertical_profile_retrievals_for_Mars_Year_34-35/13580336/1 doi: 10.21954/ou.rd.13580336.v1

Patel, M. R., Antoine, P., Mason, J., Leese, M., Hathi, B., Stevens, A. H., ... Lopez-Moreno, J. J. (2017). NOMAD spectrometer on the ExoMars trace gas orbiter mission: part 2—design, manufacturing, and testing of the ultraviolet and visible channel. *Applied Optics*, *56*(10), 2771–2782. Retrieved 2017-04-05, from http://oro.open.ac.uk/49024/

Patel, M. R., Sellers, G., Mason, J. P., Brown, M. A. J., Lewis, S. R., Rajendran, K., ... Lopez-Moreno, J. J. (2021). ExoMars TGO/NOMAD-UVIS vertical profiles of ozone: Part 1 - Seasonal variation and comparison to water. *Journal of Geophysical Research (Planets)*, *in revision*.

Quémerais, E., Bertaux, J.-L., Korablev, O., Dimarellis, E., Cot, C., Sandel, B. R., & Fussen, D. (2006). Stellar occultations observed by SPICAM on Mars Express. *Journal of Geophysical Research: Planets*, *111*(E9). Retrieved 2021-03-15, from https://agupubs.onlinelibrary.wiley.com/doi/abs/10.1029/2005JE002604 (_eprint: https://agupubs.onlinelibrary.wiley.com/doi/pdf/10.1029/2005JE002604) doi: https://doi.org/10.1029/2005JE002604

Rodgers, C. D. (2000). *Inverse Methods For Atmospheric Sounding: Theory And Practice*. World Scientific. (Google-Books-ID: Xv7sCgAAQBAJ)

Smith, M. D. (2008, May). Spacecraft Observations of the Martian Atmosphere. *Annual Review of Earth and Planetary Sciences*, *36*, 191–219. Retrieved 2017-03-28, from http://adsabs.harvard.edu/abs/2008AREPS..36..191S doi: 10.1146/annurev.earth.36.031207.124334

Smith, M. D. (2009, August). THEMIS observations of Mars aerosol optical depth from 2002–2008. *Icarus*, *202*(2), 444–452. Retrieved 2021-03-08, from https://www.sciencedirect.com/science/article/pii/S0019103509001365 doi: 10.1016/j.icarus.2009.03.027

Smith, M. D., Wolff, M. J., Clancy, R. T., Kleinböhl, A., & Murchie, S. L. (2013). Vertical distribution of dust and water ice aerosols from CRISM limb-geometry observations. *Journal of Geophysical Research: Planets*, *118*(2), 321–334. Retrieved 2021-03-08, from https://agupubs.onlinelibrary.wiley.com/doi/abs/10.1002/jgre.20047 (_eprint: https://agupubs.onlinelibrary.wiley.com/doi/pdf/10.1002/jgre.20047) doi: https://doi.org/10.1002/jgre.20047

Spiga, A., González-Galindo, F., López-Valverde, M.-A., & Forget, F. (2012). Gravity waves, cold pockets and CO2 clouds in the Martian mesosphere. *Geophysical Research Letters*, *39*(2). Retrieved 2021-03-08, from https://agupubs.onlinelibrary.wiley.com/doi/abs/10.1029/2011GL050343 (_eprint: https://agupubs.onlinelibrary.wiley.com/doi/pdf/10.1029/2011GL050343) doi: https://doi.org/10.1029/2011GL050343

Stcherbinine, A., Vincendon, M., Montmessin, F., Wolff, M. J., Korablev, O., Fedorova, A., ... Shakun, A. (2020). Martian Water Ice Clouds During the 2018 Global Dust Storm as Observed by the ACS-MIR Channel Onboard the Trace Gas Orbiter. *Journal of Geophysical Research: Planets*, *125*(3), e2019JE006300. Retrieved 2021-03-08, from https://agupubs.onlinelibrary.wiley.com/doi/abs/10.1029/2019JE006300 (_eprint: https://agupubs.onlinelibrary.wiley.com/doi/pdf/10.1029/2019JE006300) doi: https://doi.org/10.1029/2019JE006300

Steele, L. J., Lewis, S. R., & Patel, M. R. (2014, July). The radiative impact of water ice clouds from a reanalysis of Mars Climate Sounder data. *Geophysical Research Letters*, *41*(13), 4471–4478. Retrieved 2017-03-09, from http://onlinelibrary.wiley.com/doi/10.1002/2014GL060235/abstract doi: 10.1002/2014GL060235

Streeter, P., Holmes, J., Lewis, S., & Patel, M. (2021, Sep). *Mars global cli-*

mate model output masked to uvis aerosol opacity profiles, mars year 34-35. The Open University. Retrieved from https://ordo.open.ac.uk/articles/dataset/Mars_Global_Climate_Model_output_masked_to_UVIS_aerosol_opacity_profiles_Mars_Year_34-35/16616680/1 doi: 10.21954/ou.rd.16616680.v1

Streeter, P. M., Lewis, S. R., Patel, M. R., Holmes, J. A., & Kass, D. M. (2020). Surface Warming During the 2018/Mars Year 34 Global Dust Storm. *Geophysical Research Letters*, *47*(9), e2019GL083936. Retrieved 2020-05-17, from https://agupubs.onlinelibrary.wiley.com/doi/abs/10.1029/2019GL083936 (_eprint: https://agupubs.onlinelibrary.wiley.com/doi/pdf/10.1029/2019GL083936) doi: 10.1029/2019GL083936

Toon, O. B., McKay, C. P., Ackerman, T. P., & Santhanam, K. (1989). Rapid calculation of radiative heating rates and photodissociation rates in inhomogeneous multiple scattering atmospheres. *Journal of Geophysical Research: Atmospheres*, *94*(D13), 16287–16301. Retrieved 2019-08-12, from https://agupubs.onlinelibrary.wiley.com/doi/abs/10.1029/JD094iD13p16287 doi: 10.1029/JD094iD13p16287

Vandaele, A. C., Neefs, E., Drummond, R., Thomas, I. R., Daerden, F., Lopez-Moreno, J. J., ... Wolff, M. (2015, December). Science objectives and performances of NOMAD, a spectrometer suite for the ExoMars TGO mission. *Planetary and Space Science*, *119*, 233–249. Retrieved 2017-03-09, from http://www.sciencedirect.com/science/article/pii/S0032063315003025 doi: 10.1016/j.pss.2015.10.003

Vincendon, M., Pilorget, C., Gondet, B., Murchie, S., & Bibring, J.-P. (2011). New near-IR observations of mesospheric CO2 and H2O clouds on Mars. *Journal of Geophysical Research: Planets*, *116*(E11). Retrieved 2021-03-23, from https://agupubs.onlinelibrary.wiley.com/doi/abs/10.1029/2011JE003827 (_eprint: https://agupubs.onlinelibrary.wiley.com/doi/pdf/10.1029/2011JE003827) doi: https://doi.org/10.1029/2011JE003827

Wang, C., Forget, F., Bertrand, T., Spiga, A., Millour, E., & Navarro, T. (2018). Parameterization of Rocket Dust Storms on Mars in the LMD Martian GCM: Modeling Details and Validation. *Journal of Geophysical Research: Planets*, *123*(4), 982–1000. Retrieved 2020-04-01, from https://agupubs.onlinelibrary.wiley.com/doi/abs/10.1002/2017JE005255 doi: 10.1002/2017JE005255

Wang, H., & Ingersoll, A. P. (2002). Martian clouds observed by Mars Global Surveyor Mars Orbiter Camera. *Journal of Geophysical Research: Planets*, *107*(E10), 8–1–8–16. Retrieved 2021-03-08, from https://agupubs.onlinelibrary.wiley.com/doi/abs/10.1029/2001JE001815 (_eprint: https://agupubs.onlinelibrary.wiley.com/doi/pdf/10.1029/2001JE001815) doi: https://doi.org/10.1029/2001JE001815

Wolff, M. J., Smith, M. D., Clancy, R. T., Arvidson, R., Kahre, M., Seelos, F., ... Savijärvi, H. (2009, June). Wavelength dependence of dust aerosol single scattering albedo as observed by the Compact Reconnaissance Imaging Spectrometer. *Journal of Geophysical Research (Planets)*, *114*, E00D04. Retrieved 2017-04-12, from http://adsabs.harvard.edu/abs/2009JGRE..114.0D04W doi: 10.1029/2009JE003350

Wolff, M. J., Smith, M. D., Clancy, R. T., Spanovich, N., Whitney, B. A., Lemmon, M. T., ... Squyres, S. W. (2006). Constraints on dust aerosols from the Mars Exploration Rovers using MGS overflights and Mini-TES. *Journal of Geophysical Research: Planets*, *111*(E12), n/a–n/a. Retrieved from http://dx.doi.org/10.1029/2006JE002786 doi: 10.1029/2006JE002786

Zurek, R. W., & Smrekar, S. E. (2007). An overview of the Mars Re-

connaissance Orbiter (MRO) science mission. *Journal of Geophysical Research: Planets*, *112*(E5). Retrieved 2020-11-03, from https://agupubs.onlinelibrary.wiley.com/doi/abs/10.1029/2006JE002701%4010.1002/%28ISSN%292169-9100.MARSROM1 (_eprint: https://agupubs.onlinelibrary.wiley.com/doi/pdf/10.1029/2006JE002701) doi: 10.1029/2006JE002701